

# Measurement-free fault-tolerant logical zero-state encoding of the distance-three nine-qubit surface code in a one-dimensional qubit array

Hayato Goto, Yinghao Ho, and Taro Kanao

*Frontier Research Laboratory, Corporate Research & Development Center,  
Toshiba Corporation, 1, Komukai Toshiba-cho, Saiwai-ku, Kawasaki-shi, 212-8582, Japan*

(Dated: June 2, 2023)

Generation of logical zero states encoded with a quantum error-correcting code is the first step for fault-tolerant quantum computation, but requires considerably large resource overheads in general. To reduce such overheads, we propose an efficient encoding method for the distance-three, nine-qubit surface code and show its fault tolerance. This method needs no measurement, unlike other fault-tolerant encoding methods. Moreover, this is applicable to a one-dimensional qubit array. Observing these facts, we experimentally demonstrate the logical zero-state encoding of the surface code using a superconducting quantum computer on the cloud. We also experimentally demonstrate the suppression of fast dephasing due to intrinsic residual interactions in this machine by a dynamical decoupling technique dedicated for the qubit array. To extend this method to larger codes, we also investigate the concatenation of the surface code with itself, resulting in a distance-nine, 81-qubit code. We numerically show that fault-tolerant encoding of this large code can be achieved by appropriate error detection. Thus, the proposed encoding method will provide a new way to low-overhead fault-tolerant quantum computation.

## I. INTRODUCTION

Quantum computers are notoriously prone to errors due to decoherence and nonideal gate operations. To suppress these errors and perform quantum algorithms for, e.g., prime factoring [1, 2] and quantum chemistry calculations [3, 4], fault-tolerant quantum computation (FTQC) using quantum error-correcting codes [5–8] is highly expected. However, the FTQC in general requires large computational resource overheads [9–11], which is the case even for the first step in FTQC, namely, preparation of logical zero states encoded with a quantum error-correcting code. Hence, the reduction of such overheads for logical-qubit state preparation is highly desirable.

For example, an efficient fault-tolerant method for preparation of logical qubit states has been proposed for the Steane seven-qubit code (one of the smallest distance-three codes capable of correcting arbitrary single-qubit errors) [12], which has enabled experimental realization of the Steane-code logical qubit states, including so-called magic states [13–16], using laser-cooled trapped ions [17, 18]. However, the method still requires an ancilla qubit and its measurement to achieve its fault tolerance.

In this paper, we propose an efficient fault-tolerant logical zero-state encoding method for the nine-qubit surface code [19, 20], which is another small distance-three code. Remarkably, this method needs no ancilla qubit and no measurement [21, 22], which is in contrast to the conventional surface-code encoding method repeating syndrome measurements realized in recent experiments [23–25]. Moreover, the proposed method is applicable to a one-dimensional qubit array, which allows us to experimentally demonstrate this method using a su-

perconducting quantum computer on the cloud. (Interestingly, a measurement-free fault-tolerant zero-state encoding method has recently been proposed for the Steane code [26]. Unlike the proposed method, however, this needs two ancilla qubits and a Toffoli gate, and also cannot be realized in a one-dimensional qubit array.)

To extend the proposed method to larger codes, we also investigate the distance-nine, 81-qubit code obtained by concatenating the nine-qubit surface code with itself. We numerically show that fault-tolerant logical zero-state encoding of this large code can be achieved by three level-1 error-detecting teleportations [27–29], where soft-decision decoding based on conditional probability calculations [29–31] is essential for high performance. Because of the assumption of arbitrary two-qubit gates, the experimental realization of this encoding is challenging for superconducting quantum computers, but will be possible for recently developed neutral-atom quantum computers using optical tweezers [32, 33].

## II. MEASUREMENT-FREE FAULT-TOLERANT LOGICAL ZERO-STATE ENCODING OF THE NINE-QUBIT SURFACE CODE

The proposed encoding method for the nine-qubit surface code is summarized in Fig. 1, where Fig. 1a shows the definition of the code, Figs. 1b and 1c show the proposed method, and Fig. 1d shows how the stabilizers of the nine-qubit state change during the encoding [34]. The final stabilizers in Fig. 1d are exactly the same as those of the logical zero state,  $|0\rangle_L$ , encoded with the nine-qubit surface code (see Fig. 1a). This means that the proposed method can successfully encode  $|0\rangle_L$ . Also note that this encoding needs no ancilla qubit and no measurement, as mentioned above.

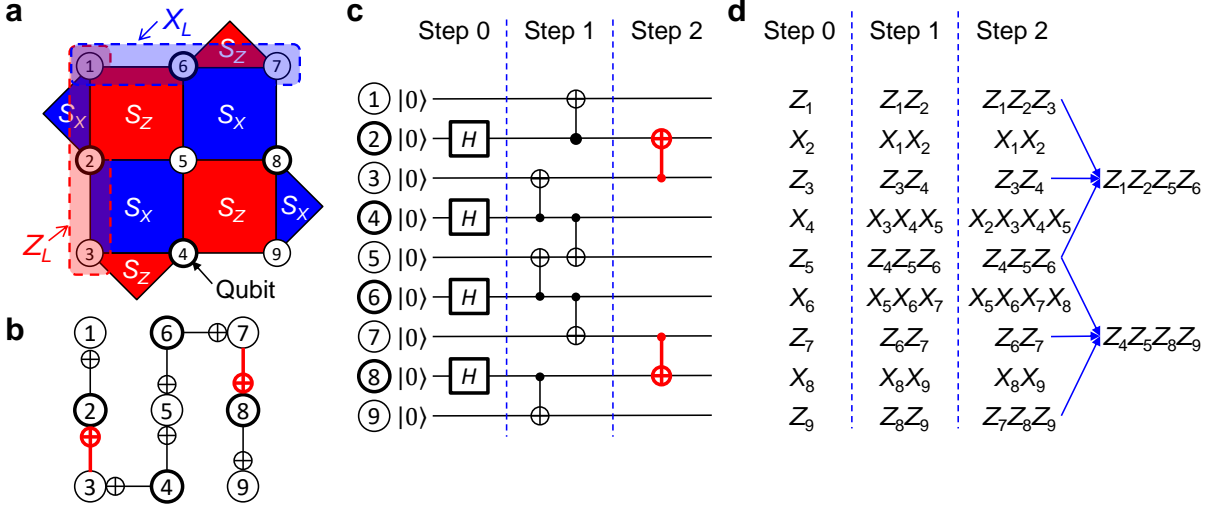


FIG. 1. Measurement-free fault-tolerant logical zero-state encoding of the nine-qubit surface code. **a** Definition of the nine-qubit surface code.  $S_Z$  and  $S_X$  denote its  $Z$  stabilizers ( $Z_6Z_7, Z_1Z_2Z_5Z_6, Z_4Z_5Z_8Z_9, Z_3Z_4$ ) and  $X$  stabilizers ( $X_1X_2, X_2X_3X_4X_5, X_5X_6X_7X_8, X_8X_9$ ), respectively.  $Z_L = Z_1Z_2Z_3$  and  $X_L = X_1X_6X_7$  are its logical Pauli operators. The logical zero state  $|0\rangle_L$  is the simultaneous eigenstate of the eight stabilizers and  $Z_L$  with eigenvalues of 1. **b** Graphical description of the proposed method. Bold circles indicate that the corresponding qubits are initialized to  $|+\rangle = H|0\rangle = (|0\rangle + |1\rangle)/\sqrt{2}$ , where  $H$  denotes the Hadamard gate, and the others are to  $|0\rangle$ . Two bold CNOT gates in red are performed after the other six CNOT gates. **c** Quantum circuit corresponding to **b**. **d** Nine stabilizers describing the nine-qubit state at the end of each step in **c**.

The fault tolerance of the method is explained as follows. At the end of Step 1 in Fig. 1c, the weights (the numbers of non-identity Pauli operators) of all the nine stabilizers are two or three, as shown in Fig. 1d, which allows us to regard any correlated  $X$  and  $Z$  errors induced by the six controlled-NOT (CNOT) gates in Step 1 as single-qubit  $X$  and  $Z$  errors, respectively. (In this work, we assume that correlated errors occur only by two-qubit gates.) Hence, we have only to care correlated errors induced by the two CNOT gates in Step 2. (A similar technique is used for the above-mentioned method for the Steane code [12].) The correlated errors are  $X_2X_3$  and  $X_7X_8$ , which can be corrected by this code [35]. Thus, this encoding induces no uncorrelatable errors up to the first order of physical error rates, which means its fault tolerance.

### III. EXPERIMENTAL DEMONSTRATION OF THE PROPOSED SURFACE-CODE ENCODING

Observing that the proposed encoding can be realized using a one-dimensional qubit array, as shown in Fig. 1b, we did experiments of this encoding using a superconducting quantum computer on the cloud (27-qubit *ibm-kawasaki* [36]), the qubit layout of which is shown in Fig. 2. We used nine qubits in a row among the 27 qubits, which are highlighted in Fig. 2. The performance of this machine is summarized in Tables I and II.

First, we prepare  $|0\rangle_L$  according to the quantum circuit in Fig. 1c and measure  $Z$  of all the qubits after a

delay time from the preparation. We decode the measurement results using the hard-decision decoding rule in Appendix A, and estimate the measurement result of  $Z_L$ . If the decoding results in  $Z_L = -1$ , the decoding fails, which means a logical error.

The experimental results are shown in Figure 3a, where  $p_L$  (circles) is the logical error probability,  $p_C$  (triangles) is the conditional logical error probability under the condition that all the four  $Z$  stabilizers are 1, and  $p_Z$  (squares) is the no- $X$ -error probability that both  $Z_L$  and the four  $Z$  stabilizers are 1.  $p_L$  and  $p_C$  are substantially lower than  $1 - p_Z$ . In particular,  $p_L$  and  $p_C$  are about 0.5% and 0.004%, respectively, at the zero delay time, which are, respectively, lower and much lower than physical-CNOT error rates (see Table I). These re-

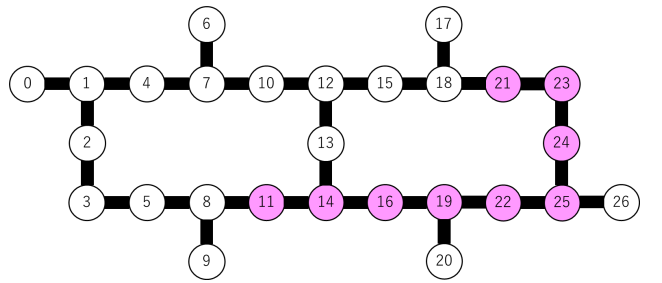


FIG. 2. Qubit layout of the superconducting quantum computer used in this work. This is 27-qubit *ibm-kawasaki* [36]. Qubits 21, 23, 24, 25, 22, 19, 16, 14, and 11 in this machine are used for Qubits 1–9 in Fig. 1.

TABLE I. **CNOT-gate performance of 27-qubit ibm-kawasaki.** “CNOT” column shows the control-qubit (C) and target-qubit (T) numbers of this machine (see Fig. 2).

CNOT	Error rate (%)	Gate time (ns)
C21, T23	0.51	292
C23, T24	0.82	427
C24, T25	0.58	363
C25, T22	0.68	284
C22, T19	0.88	281
C19, T16	0.88	295
C16, T14	0.54	295
C14, T11	2.26	409

TABLE II. **Qubit coherence times of 27-qubit ibm-kawasaki [37].** “Qubit” column shows the qubit number of this machine (see Fig. 2).

Qubit	$T_1$ ( $\mu$ s)	$T_2$ ( $\mu$ s)
Q21	144	108
Q23	134	332
Q24	169	125
Q25	174	213
Q22	147	188
Q19	196	263
Q16	128	133
Q14	122	78
Q11	113	110

sults indicates that  $|0\rangle_L$  was successfully prepared and its logical error probability could be suppressed by error correction or detection.

Note that the above results depend only on  $Z$  measurements (measurements of bit-string states) and provide no information of  $X$  measurements (quantum superpositions of bit-string states). The logical zero state,  $|0\rangle_L$ , encoded with the nine-qubit surface code is a quantum superposition of 16 bit-string states satisfying the five  $Z$ -stabilizer conditions. To evaluate the quantum superposition in the prepared  $|0\rangle_L$ , we also measured the  $X$  stabilizers, the results of which are shown by squares in Fig. 3b. When the delay time is zero, the no- $Z$ -error probability,  $p_X$ , that all the four  $X$  stabilizers are 1 is 79%. (The corresponding value of  $p_Z$  is 87%, as found in Fig 3a.) This result suggests that the prepared  $|0\rangle_L$  was actually a quantum superposition of bit-string states, as expected. In fact, it is shown that the fidelity of the prepared  $|0\rangle_L$  is lower bounded by  $p_Z + p_X - 1 = 0.66$  (see Appendix C), which is substantially higher than that for the maximally mixed state of the 16 bit-string states, namely,  $1/16 = 0.0625$ . (This fidelity evaluation of  $|0\rangle_L$  prepared by the proposed method would be useful for benchmarking of real quantum computers with at least nine qubits in a row.)

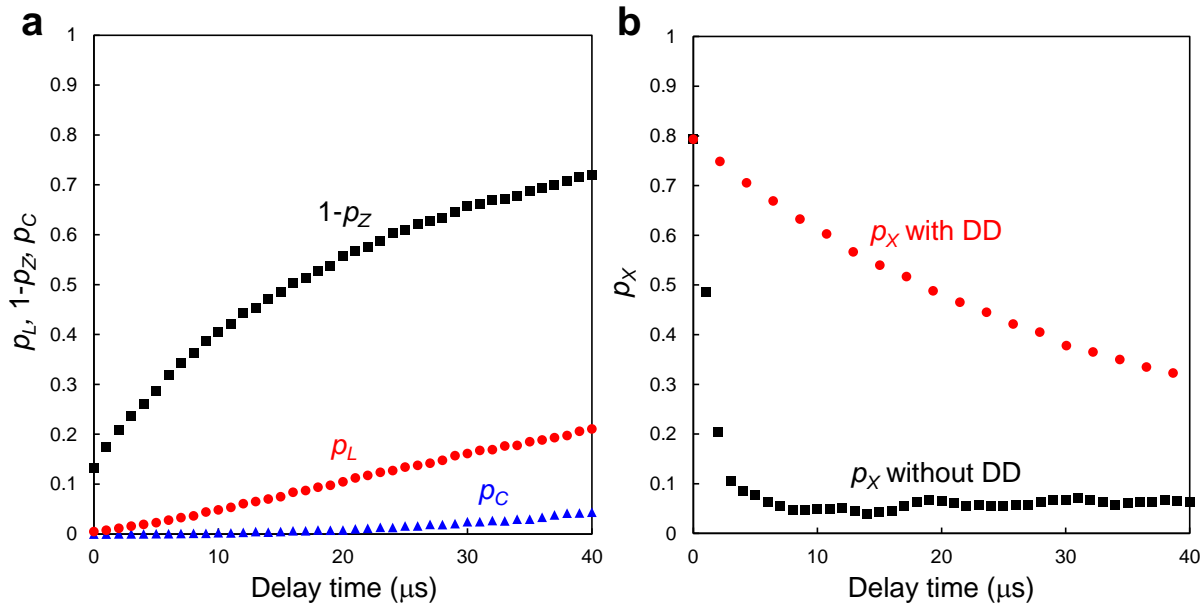


FIG. 3. **Experimental results of the logical zero-state encoding of the nine-qubit surface code using a superconducting quantum computer.** **a** Delay-time dependence of the logical error probability  $p_L$  (circles), the conditional logical error probability  $p_C$  (triangles) under the condition that all the four  $Z$  stabilizers are 1, and the no- $X$ -error probability  $p_Z$  (squares) that both  $Z_L$  and the four  $Z$  stabilizers are 1. **b** Delay-time dependence of the no- $Z$ -error probability  $p_X$  that all the four  $X$  stabilizers are 1. The circles and squares show the results, respectively, with and without the dynamical decoupling (DD) technique shown in Fig. 4. In both **a** and **b**, statistical errors are negligible compared to symbol sizes.

#### IV. DYNAMICAL DECOUPLING TO SUPPRESS DEPHASING DUE TO RESIDUAL ZZ INTERACTIONS

It is notable that  $p_X$  decays much faster than  $p_Z$ . (The recovery of  $p_X$  to  $1/2^4 = 0.0625$  found in Fig. 3b can be explained by convergence to a maximally mixed state of the 16 bit-string states due to decoherence.) Since this decay of  $p_X$  is too fast compared to qubit coherence times (see Table II), the decay may be caused by another decoherence source. We identify it with so-called residual ZZ interactions inducing unwanted additional phase rotation only for  $|11\rangle$  of adjacent qubits. To suppress this dephasing due to the ZZ interactions, we applied a dynamical decoupling technique dedicated for the qubit array, which is shown in Fig. 4. (Similar studies with different techniques have been reported [38, 39].) The results are shown by circles in Fig. 3b, which clearly shows that the decay of  $p_X$  becomes substantially slower, as expected. This concludes that the fast decay of  $p_X$  is due to the ZZ interactions in this machine, and this can be suppressed by the proposed dynamical decoupling technique in Fig. 4.

#### V. FAULT-TOLERANT LOGICAL ZERO-STATE ENCODING OF THE CONCATENATED NINE-QUBIT SURFACE CODE

The proposed encoding method is applicable only to the distance-three, nine-qubit surface code, which is small for practical applications [9–11]. To extend the proposed method to larger codes, we consider the con-

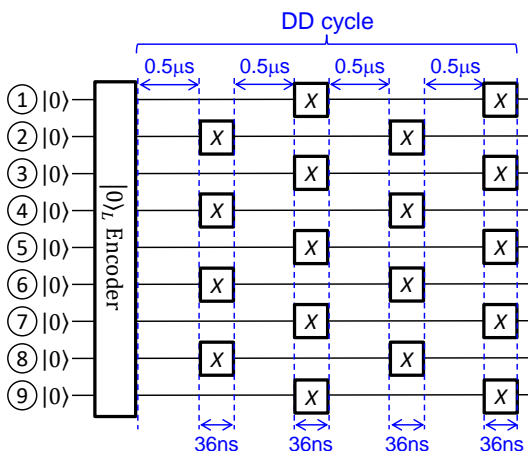


FIG. 4. **Dynamical decoupling technique for suppressing dephasing in  $|0\rangle_L$  due to ZZ interactions.** Each dynamical decoupling (DD) cycle consists of four  $0.5\text{-}\mu\text{s}$  delay times (more precisely,  $0.5013\ \mu\text{s}$ ) followed by four or five X gates with gate times of  $36\ \text{ns}$  (more precisely,  $35.6\ \text{ns}$ ). Thus, each DD cycle takes  $2.1476\ \mu\text{s}$ . It can easily be shown that this DD cycle can eliminate unwanted additional phase rotations due to ZZ interactions.

catenation of the nine-qubit surface code with itself [5], which leads to the distance-nine, 81-qubit code.

The logical zero state,  $|0\rangle_{L2}$ , encoded with the concatenated code can be generated straightforwardly by the quantum circuit in Fig. 1c, where the physical zero states, physical Hadamard gates, and physical CNOT gates are, respectively, replaced by the encoded zero states  $|0\rangle_{L1}$ , encoded Hadamard gates, and encoded CNOT gates for the nine-qubit surface code, where the subscripts L2 and L1 denote the concatenation levels [27–29]. The fault-tolerant preparation of  $|0\rangle_{L1}$  can be done by the proposed method explained in Sec. II. The encoded Hadamard gate can be implemented fault-tolerantly by the transversal Hadamard gate [5],  $H_1H_2H_3H_4H_5H_6H_7H_8H_9$ , followed by renumbering ( $90^\circ$  rotating) the qubits as  $1 \rightarrow 7$ ,  $2 \rightarrow 6$ ,  $3 \rightarrow 1$ ,  $4 \rightarrow 2$ ,  $9 \rightarrow 3$ ,  $8 \rightarrow 4$ ,  $7 \rightarrow 9$ , and  $6 \rightarrow 8$ . The encoded CNOT gate can also be implemented fault-tolerantly by the transversal CNOT gate [5, 19].

To evaluate the performance of the straightforward encoding of  $|0\rangle_{L2}$ , we numerically simulate it and evaluate its logical error probability  $p_{L2}$  using Z measurement results. This simulation is based on the stabilizer simulation [40]. In this simulation, we assume the error model where errors occur only in physical CNOT gates, which is modeled in a standard manner, that is, a physical CNOT gate is modeled by an ideal CNOT gate followed by one of 15 two-qubit Pauli errors with equal probability of  $p_{\text{CNOT}}/15$  [27–29]. For the decoding of the concatenated code, we use soft-decision decoding based on conditional probability calculations [29–31] (see Appendix B), which is important to achieve almost optimal performance.

The simulation results are shown by circles in Fig. 5a. Although the logical error probability can become lower than the physical error probability, its exponent of about 3 is smaller than that expected from the code distance of 9, namely, 5. (In general, distance-nine codes can, in principle, correct four arbitrary independent qubit errors, leading to the exponent of 5.)

To improve the performance, error detection followed by postselection (restarting from the beginning if errors are detected until no errors are detected) is effective. We perform level-1 error-detecting teleportations (EDTs) [27–29] on the level-1 Qubits 2, 5, and/or 8 after the above straightforward generation of  $|0\rangle_{L2}$ . The simulation results are shown in Fig 5a. When the EDT is performed only on Qubit 5, the logical error probability becomes lower, but the exponent is still about 3. When the EDT is performed on Qubits 2 and 8, the logical error probability is reduced by two orders of magnitude, and also the exponent is increased to about 4 but still smaller than 5. When the EDT is performed on Qubits 2, 5 and 8, not only the logical error probability becomes further lower, but also the exponent exceeds 5. (Note that the hard-decision decoding for the concatenated code can, in principle, achieve the exponent up to 4, and therefore the present result achieving the exponent of 5 clearly shows the advantage of the soft-decision decoding.) Thus, it has turned out that EDTs on Qubits 2, 5, and 8 are

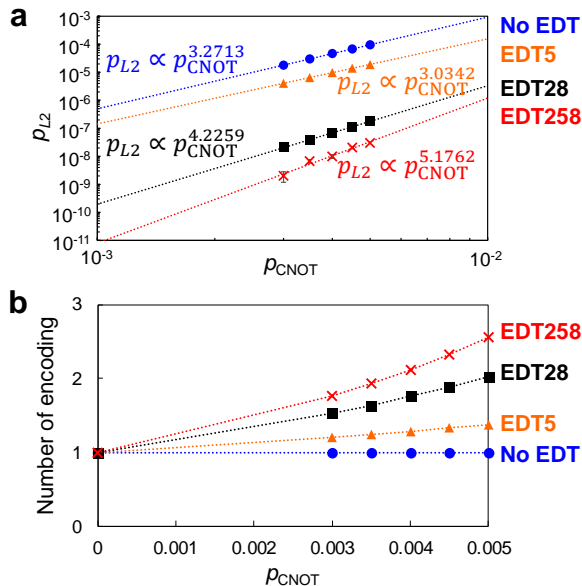


FIG. 5. **Simulation results of the logical zero-state encoding of the concatenated code.** **a** Logical error probabilities. The circles, triangles, squares, and crosses show, respectively, the results for encoding without error-detecting teleportations (EDTs), with an EDT on the level-1 Qubit 5, with EDTs on the level-1 Qubits 2 and 8, and with EDTs on the level-1 Qubits 2, 5, and 8. The dotted lines and proportionality relations show fitting results with a power function. The number of repetition to estimate the probabilities is  $10^8$  for “No EDT” and “EDT5” and  $10^{10}$  for “EDT28” and “EDT258.” **b** Average total number of encoding until success. The dotted lines are eye guides. In both **a** and **b**, statistical errors are negligible compared to symbol sizes, except for “EDT258” in **a**.

enough to achieve potential performance of the concatenated code. In this case, the logical error probability is estimated around  $10^{-11}$  for  $p_{\text{CNOT}} = 10^{-3}$ , which is sufficiently low for large-scale problems. Figure 5b also shows that the increase of overheads by the EDTs and postselection will not be very large.

## VI. CONCLUSION

We have proposed a measurement-free fault-tolerant logical zero-state encoding method for the distance-three, nine-qubit surface code, and have experimentally demonstrated it using a superconducting quantum computer. The experimental results indicate that the logical zero state was successfully prepared, and its logical error probability could be suppressed by error correction or detection. We have also experimentally demonstrated that the dephasing due to residual  $ZZ$  interactions in this machine can be suppressed by the proposed dynamical decoupling technique. We have also proposed a fault-tolerant logical zero-state encoding method for the distance-nine, 81-qubit code obtained by concatenating the nine-qubit sur-

face code with itself. Because of the assumption of arbitrary two-qubit gates, this large-scale encoding is challenging for superconducting quantum computers, but will be possible for recently developed neutral-atom quantum computers with optical tweezers. Thus, the present results will provide a new way to low-overhead fault-tolerant quantum computation.

## ACKNOWLEDGMENTS

We acknowledge the use of IBM Quantum services for experiments in this work. The views expressed are those of the authors, and do not reflect the official policy or position of IBM or the IBM Quantum team. The use of IBM’s superconducting quantum computer on the cloud was supported by UTokyo Quantum Initiative.

### Appendix A: Hard-decision decoding of the nine-qubit surface code

We estimate the  $X$  errors in  $|0\rangle_L$  as follows. We first calculate the measurement results of the  $Z$  stabilizers as

$$s_1 = m_6 m_7, \quad (\text{A1})$$

$$s_2 = m_1 m_2 m_5 m_6, \quad (\text{A2})$$

$$s_3 = m_4 m_5 m_8 m_9, \quad (\text{A3})$$

$$s_4 = m_3 m_4, \quad (\text{A4})$$

where  $m_j$  denotes the measurement result of  $Z_j$ . Next, we estimate the  $X$  errors according to Table III. Finally, we flip the measurement results  $\{m_j\}$  according to the estimated  $X$  errors. Then, the value of  $Z_L$  is estimated at  $m_1 m_2 m_3$  after the flips.

TABLE III.  **$X$ -error estimation from  $Z$  measurement results.** Measurement results of the  $Z$  stabilizers,  $s_1$ – $s_4$ , are defined by Eqs. (A1)–(A4).

$s_1$	$s_2$	$s_3$	$s_4$	$X$ errors
+1	+1	+1	+1	No error
-1	+1	+1	+1	$X_7$
+1	-1	+1	+1	$X_2$
+1	+1	-1	+1	$X_8$
+1	+1	+1	-1	$X_3$
-1	-1	+1	+1	$X_6$
-1	+1	-1	+1	$X_7 X_8$
-1	+1	+1	-1	$X_3 X_7$
+1	-1	-1	+1	$X_5$
+1	-1	+1	-1	$X_2 X_3$
+1	+1	-1	-1	$X_4$
-1	-1	-1	+1	$X_5 X_7$
-1	-1	+1	-1	$X_3 X_6$
-1	+1	-1	-1	$X_4 X_7$
+1	-1	-1	-1	$X_3 X_5$
-1	-1	-1	-1	$X_4 X_6$

## Appendix B: Soft-decision decoding of the concatenated nine-qubit surface code

First, the soft-decision decoding rule for the nine-qubit surface code is given as follows [29, 31]:

$$P^{(1)}(z) = \frac{R^{(1)}(z)}{R^{(1)}(1) + R^{(1)}(-1)}, \quad (\text{B1})$$

$$R^{(1)}(z) = \sum_{z_1=\pm 1} \sum_{z_2=\pm 1} \sum_{z_3=\pm 1} \sum_{z_4=\pm 1} \sum_{z_5=\pm 1} \sum_{z_6=\pm 1} \sum_{z_7=\pm 1} \sum_{z_8=\pm 1} \sum_{z_9=\pm 1} P_1^{(0)}(z_1)P_2^{(0)}(z_2)P_3^{(0)}(z_3)P_4^{(0)}(z_4)P_5^{(0)}(z_5)P_6^{(0)}(z_6) \\ \times P_7^{(0)}(z_7)P_8^{(0)}(z_8)P_9^{(0)}(z_9)\delta(z_1z_2z_3 = z)\delta(z_6z_7 = 1)\delta(z_1z_2z_5z_6 = 1)\delta(z_4z_5z_8z_9 = 1)\delta(z_3z_4 = 1), \quad (\text{B2})$$

where  $P^{(1)}(z)$  is the probability that the level-1  $Z_L$  has the value of  $z$ ,  $R^{(1)}(z)$  is the corresponding relative probability,  $z_j$  denotes the correct value of  $Z_j$  for the  $j$ th physical qubit,  $P_j^{(0)}(z_j)$  is the corresponding probability, and the  $\delta(\text{condition})$  is the indicator function taking 1 if the condition is true and otherwise 0. Assuming equal physical-qubit error probability of  $p_e$ , we have

$$P_j^{(0)}(m_j) = 1 - p_e, \quad P_j^{(0)}(-m_j) = p_e, \quad (\text{B3})$$

where  $m_j$  is the measurement result of  $Z_j$ . In this work, we set  $p_e$  to 0.01. (The soft-decision decoding is insensitive to the setting of  $p_e$  [29].) Thus, we can obtain  $P^{(1)}(z)$  using the measurement results  $\{m_j\}$ .

Next, the soft-decision decoding rule for the concatenated code is given similarly as follows [29, 31]:

$$P^{(2)}(z) = \frac{R^{(2)}(z)}{R^{(2)}(1) + R^{(2)}(-1)}, \quad (\text{B4})$$

$$R^{(2)}(z) = \sum_{z_1=\pm 1} \sum_{z_2=\pm 1} \sum_{z_3=\pm 1} \sum_{z_4=\pm 1} \sum_{z_5=\pm 1} \sum_{z_6=\pm 1} \sum_{z_7=\pm 1} \sum_{z_8=\pm 1} \sum_{z_9=\pm 1} P_1^{(1)}(z_1)P_2^{(1)}(z_2)P_3^{(1)}(z_3)P_4^{(1)}(z_4)P_5^{(1)}(z_5)P_6^{(1)}(z_6) \\ \times P_7^{(1)}(z_7)P_8^{(1)}(z_8)P_9^{(1)}(z_9)\delta(z_1z_2z_3 = z)\delta(z_6z_7 = 1)\delta(z_1z_2z_5z_6 = 1)\delta(z_4z_5z_8z_9 = 1)\delta(z_3z_4 = 1), \quad (\text{B5})$$

where  $P^{(2)}(z)$  is the probability that the level-2  $Z_L$  has the value of  $z$ ,  $R^{(2)}(z)$  is the corresponding relative probability,  $z_j$  denotes the correct value of the level-1  $Z_L$  for the  $j$ th level-1 encoded qubit,  $P_j^{(1)}(z_j)$  is the corresponding probability obtained from the measurement results as explained above.

Thus, we estimate the value of the level-2  $Z_L$  at 1 if  $P^{(2)}(1) > P^{(2)}(-1)$ , otherwise at  $-1$ .

## Appendix C: Fidelity estimation of the experimentally prepared $|0\rangle_L$

The fidelity of the experimentally prepared  $|0\rangle_L$  is formulated as  $F_0 = \langle 0 | \rho_0 | 0 \rangle_L$ , where  $\rho_0$  denotes the density

operator describing the experimentally prepared  $|0\rangle_L$ . In the following, we show that  $F_0 \geq p_Z + p_X - 1$ .

Consider two bits,  $b_Z$  and  $b_X$ , defined as  $b_Z = 0$  if all the five  $Z$  stabilizers of  $|0\rangle_L$  are 1, otherwise  $b_Z = 1$ , and  $b_X = 0$  if all the four  $X$  stabilizers of  $|0\rangle_L$  are 1, otherwise  $b_X = 1$ . We also denote the probability of  $(b_Z, b_X)$  by  $P_b(b_Z, b_X)$ . Then, we have  $F_0 = P_b(0, 0)$ ,  $p_Z = P_b(0, 0) + P_b(0, 1)$ , and  $p_X = P_b(0, 0) + P_b(1, 0)$ . We also have  $P_b(0, 0) + P_b(1, 0) + P_b(0, 1) + P_b(1, 1) = 1$ . Using these relations, we can easily obtain the desired result:

$$F_0 = p_Z + p_X - 1 + P_b(1, 1) \geq p_Z + p_X - 1. \quad (\text{C1})$$

- 
- [1] P. W. Shor, Algorithms for Quantum Computation: Discrete Logarithms and Factoring, in Proceedings of the 35th Annual Symposium on Foundations of Computer Science, Santa Fe, 1994, (IEEE, 1994), p. 124.
- [2] A. Ekert and R. Jozsa, Quantum Computation and Shor's factoring algorithm, *Rev. Mod. Phys.* **68**, 733–753 (1996).

- [3] A. Aspuru-Guzik, A. D. Dutoi, P. J. Lovec, and M. Head-Gordona, Simulated Quantum Computation of Molecular Energies, *Science* **309**, 1704–1707 (2005).
- [4] S. McArdle, S. Endo, A. Aspuru-Guzik, S. C. Benjamin, and X. Yuan, Quantum computational chemistry, *Rev. Mod. Phys.* **92**, 015003 (2020).
- [5] M. A. Nielsen and I. L. Chuang, *Quantum Computation and Quantum Information* (Cambridge Univ. Press,

- Cambridge, 2000).
- [6] P. W. Shor, Fault-tolerant quantum computation, in Proc. 37th Symp. on Foundations of Computer Science 56–65 (IEEE Computer Soc. Press, Los Alamitos, CA, 1996).
- [7] D. Gottesman, Theory of fault-tolerant quantum computation, Phys. Rev. A **57**, 127 (1998).
- [8] E. Knill, R. Laflamme, and W. H. Zurek, Resilient Quantum Computation, Science **279**, 342 (1998).
- [9] N. C. Jones, R. Van Meter, A. G. Fowler, P. L. McMahon, J. Kim, T. D. Ladd, and Y. Yamamoto, Layered Architecture for Quantum Computing, Phys. Rev. X **2**, 031007 (2012).
- [10] A. G. Fowler, M. Mariantoni, J. M. Martinis, and A. N. Cleland, Surface codes: Towards practical large-scale quantum computation, Phys. Rev. A **86**, 032324 (2012).
- [11] C. Gidney and M. Ekerå, How to factor 2048 bit RSA integers in 8 hours using 20 million noisy qubits, Quantum **5**, 433 (2021).
- [12] H. Goto, Minimizing resource overheads for fault-tolerant preparation of encoded states of the Steane code, Sci. Rep. **6**, 19578 (2016).
- [13] S. Bravyi and A. Kitaev, Universal quantum computation with ideal Clifford gates and noisy ancillas, Phys. Rev. A **71**, 022316 (2005).
- [14] B. W. Reichardt, Quantum Universality from Magic States Distillation Applied to CSS Codes, Quant. Inf. Proc. **4**, 251–264 (2005).
- [15] H. Goto, Step-by-step magic state encoding for efficient fault-tolerant quantum computation, Sci. Rep. **4**, 7501 (2014).
- [16] C. Chamberland and A. W. Cross, Fault-tolerant magic state preparation with flag qubits, Quantum **3**, 143 (2019).
- [17] C. Ryan-Anderson, J. G. Bohnet, K. Lee, D. Gresh, A. Hankin, J. P. Gaebler, D. Francois, A. Chernoguzov, D. Lucchetti, N. C. Brown, T. M. Gatterman, S. K. Halit, K. Gilmore, J. A. Gerber, B. Neyenhuis, D. Hayes, and R. P. Stutz, Realization of Real-Time Fault-Tolerant Quantum Error Correction, Phys. Rev. X **11**, 041058 (2021).
- [18] L. Postler, S. Heußen, I. Pogorelov, M. Rispler, T. Feldker, M. Meth, C. D. Marciniak, R. Stricker, M. Ringbauer, R. Blatt, P. Schindler, M. Müller, and T. Monz, Demonstration of fault-tolerant universal quantum gate operations, Nature (London) **605**, 675–680 (2022).
- [19] C. Horsman, A. G. Fowler, S. Devitt, and R. Van Meter, Surface code quantum computing by lattice surgery, New J. Phys. **14**, 123011 (2012).
- [20] Y. Tomita and K. M. Svore, Low-distance surface codes under realistic quantum noise, Phys. Rev. A **90**, 062320 (2014).
- [21] We have recently found a similar encoding method in Ref. 22. However, its fault tolerance has not been shown.
- [22] K. J. Satzinger, Y.-J. Liu, A. Smith, C. Knapp, M. Newman, C. Jones *et al.*, Realizing topologically ordered states on a quantum processor, Science **374**, 1237–1241 (2021).
- [23] Y. Zhao, Y. Ye, H.-L. Huang, Y. Zhang, D. Wu, H. Guan, Q. Zhu, Z. Wei, T. He, S. Cao, F. Chen, T.-H. Chung, H. Deng, D. Fan, M. Gong, C. Guo, S. Guo, L. Han, N. Li, S. Li, Y. Li, F. Liang, J. Lin, H. Qian, H. Rong, H. Su, L. Sun, S. Wang, Y. Wu, Y. Xu, C. Ying, J. Yu, C. Zha, K. Zhang, Y.-H. Huo, C.-Y. Lu, C.-Z. Peng, X. Zhu, and J.-W. Pan, Realization of an Error-Correcting Surface Code with Superconducting Qubits, Phys. Rev. Lett. **129**, 030501 (2022).
- [24] S. Krinner, N. Lacroix, A. Remm, A. Di Paolo, E. Genois, C. Leroux, C. Hellings, S. Lazar, F. Swiadek, J. Herrmann, G. J. Norris, C. K. Andersen, M. Müller, A. Blais, C. Eichler, and A. Wallraff, Realizing repeated quantum error correction in a distance-three surface code, Nature (London) **605**, 669–674 (2022).
- [25] Google Quantum AI, Suppressing quantum errors by scaling a surface code logical qubit, Nature (London) **614**, 676–681 (2023).
- [26] S. Heußen, L. Postler, M. Rispler, I. Pogorelov, C. D. Marciniak, T. Monz, P. Schindler, and M. Müller, Strategies for a practical advantage of fault-tolerant circuit design in noisy trapped-ion quantum computers, Phys. Rev. A **107**, 042422 (2023).
- [27] E. Knill, Quantum computing with realistically noisy devices, Nature (London) **434**, 39–44 (2005).
- [28] H. Goto and K. Ichimura, Fault-tolerant quantum computation with probabilistic two-qubit gates, Phys. Rev. A **80**, 040303(R) (2009).
- [29] H. Goto and H. Uchikawa, Fault-tolerant quantum computation with a soft-decision decoder for error correction and detection by teleportation, Sci. Rep. **3**, 2044 (2013).
- [30] D. Poulin, Optimal and efficient decoding of concatenated quantum block codes, Phys. Rev. A **74**, 052333 (2006).
- [31] H. Goto and H. Uchikawa, Soft-decision decoder for quantum erasure and probabilistic-gate error models, Phys. Rev. A **89**, 022322 (2014).
- [32] D. Bluvstein, H. Levine, G. Semeghini, T. T. Wang, S. Ebadi, M. Kalinowski, A. Keesling, N. Maskara, H. Pichler, M. Greiner, V. Vuletić, and M. D. Lukin, A quantum processor based on coherent transport of entangled atom arrays, Nature (London) **604**, 451–456 (2022).
- [33] T. M. Graham, Y. Song, J. Scott, C. Poole, L. Phuttitarn, K. Jooya, P. Eichler, X. Jiang, A. Marra, B. Grinkemeyer, M. Kwon, M. Ebert, J. Cherek, M. T. Lichtman, M. Gillette, J. Gilbert, D. Bowman, T. Ballance, C. Campbell, E. D. Dahl, O. Crawford, N. S. Blunt, B. Rogers, T. Noel, and M. Saffman, Multi-qubit entanglement and algorithms on a neutral-atom quantum computer, Nature (London) **604**, 457–462 (2022).
- [34] An  $n$ -qubit stabilizer state is described as a simultaneous eigenstate of  $n$  stabilizers with eigenvalues of 1 [5].
- [35] The  $X_2X_3$  error can be found by the flips of the two  $Z$  stabilizers,  $Z_1Z_2Z_5Z_6$  and  $Z_3Z_4$ , and the  $X_7X_8$  error can also be found by the flips of  $Z_6Z_7$  and  $Z_4Z_5Z_8Z_9$ . Also, there are no correlated  $Z$  errors, because  $|0\rangle_L$  has another stabilizer  $Z_L$  and consequently the weights of its  $Z$  stabilizers are still two or three after Step 2, as shown in Fig. 1d.
- [36] IBM Q: <https://quantum-computing.ibm.com/>
- [37] The larger value of  $T_2$  than  $2T_1$  for Qubit 23 is due to a calibration error in this system.
- [38] B. Pokharel, N. Anand, B. Fortman, and D. A. Lidar, Demonstration of Fidelity Improvement Using Dynamical Decoupling with Superconducting Qubits, Phys. Rev. Lett. **121**, 220502 (2018).
- [39] V. Tripathi, H. Chen, M. Khezri, K.-W. Yip, E. M. Levenson-Falk, and D. A. Lidar, Suppression of Crosstalk in Superconducting Qubits Using Dynamical Decoupling, Phys. Rev. Appl. **18**, 024068 (2022).

- [40] S. Aaronson and D. Gottesman, Improved simulation of stabilizer circuits, *Phys. Rev. A* **70**, 052328 (2004).